Electrochimica Acta 134 (2014) 266–271

Contents lists available at ScienceDirect

Electrochimica Acta

journal homepage: www.elsevier.com/locate/electacta

Nickel nanowires as effective catalysts for urea electro-oxidation

Wei Yan, Dan Wang, Luis A. Diaz, Gerardine G. Botte*

Center for Electrochemical Engineering Research, Chemical and Biomolecular Engineering Department, 165 Stocker Center, Ohio University, Athens, OH 45701

ARTICLE INFO

Article history:
Received 4 November 2013
Received in revised form 16 March 2014
Accepted 19 March 2014
Available online 23 April 2014

Keywords:
Urea electrolysis
Nickel nanowires
Hydrogen production
Wastewater remediation.

ABSTRACT

Urea electrolysis catalyzed by bulk nickel catalysts has revealed great potential in hydrogen production and remediation of urea-rich wastewater. In this study, one-dimensional (1-D) nickel nanowires electrocatalyts (NNE) were developed to enhance the electrocatalytic oxidation of urea. The nanowires were fabricated by electrodeposition assisted with an anodic aluminium oxide (AAO) template. The NNE exhibit higher electrocatalytic activity and higher current efficiency of urea electrolysis than that of bulk nickel film electrocatalysts (NFE). The as-prepared NNE represent a new class of robust catalysts for urea electrolysis, which demonstrates promise for future applications in hydrogen production, fuel cells, and wastewater remediation.

1. Introduction

A focus and concern on urea [$CO(NH_2)_2$] utilization is entirely appropriate since it had been a vital energy and environmental issue in the past five years [1–8]. Comparing with other gas/liquid hydrogen carriers, solid urea has recently been considered as a promising hydrogen carrier for sustainable energy supply due to its stable, non-toxic, and non-flammable properties as well as its convenience for hydrogen storage and transportation[1,2,4,5,7]. Furthermore, urea-rich wastewater has been regarded as a danger for both the environment and people's health [2,9–11]. Urea is employed as a nitrogen-release fertilizer and as an animal feed additive. During the industrial synthesis process of urea, however, a large amount of urea-rich wastewater is generated daily. Additionally, urea is discharged in wastewater sewage systems since urea is the major constituent of human and animal urine. The untreated urea-rich wastewater results in severe environmental contamination and human health problems as urea can naturally hydrolyze into toxic ammonia poisoning ground water and polluting air.

Urea electrolysis has proven to be an effective technology for remediation of urea-rich wastewater with the simultaneous acquisition of high-purity hydrogen. Urea electrolysis (Eqns.1- 4) can directly convert urea into valuable hydrogen and benign nitrogen and thus can effectively prevent ammonia emissions [2]. The generated carbon dioxide is absorbed in the alkaline electrolyte as a carbonate salt [2,12] serving as a carbon dioxide scrubber. The CO_2 could be removed from the electrolyte and captured if desired. In comparison with the thermodynamics cell voltage of 1.23 V required for water electrolysis, the overall cell voltage for urea electrolysis is 0.37 V at standard conditions (Eqn. 4), which means that hydrogen production from urea electrolysis theoretically consumes less energy than water electrolysis.

$$\text{Anode}: 6Ni(OH)_2 + 6OH^- \rightarrow 6NiOOH + 6H_2O + 6e^- \quad (1)$$

$$CO(NH_2)_2 + 6NiOOH + H_2O \rightarrow 6Ni(OH)_2 + N_2 + CO_2 \quad (2)$$

$$\text{Cathode}: 6H_2O + 6e^- \rightarrow 3H_2 + 6OH^- \quad (3)$$

$$\text{Overall}: CO(NH_2)_2 + H_2O \rightarrow N_2 + 3H_2 + CO_2 \quad (4)$$

Nickel has been experimentally and computationally investigated as an essential catalytic component for the urea electro-oxidation reaction [2,13–16]. The inexpensive nickel catalyst has shown higher electrocatalytic activity than noble metals, such as Pt, Ir, Rh etc., in alkaline media [2]. However, improvements of the catalytic efficiency for urea oxidation are still imperative due to the degradation of nickel catalysts suggesting an easily deactivated catalytic surface during urea electro-oxidation [17]. Incorporating noble metals into nickel catalysts showed an enhanced urea electro-oxidation current [17,18]; however, the cost of catalysts inevitably increased due to the noble metal components. Thus, finding an inexpensive, highly efficient, and stable catalyst towards urea electro-oxidation is crucial to commercialize and deploy the urea electrolysis process.

Low dimensional nanomaterials have been utilized for enhancing electrocatalytic efficiency and improving reaction rates due to their excellent and unique physical and chemical properties

* Corresponding author. Tel.: +1 740 593-9670; fax: +1 740 593-0873.
E-mail address: botte@ohio.edu (G.G. Botte).

http://dx.doi.org/10.1016/j.electacta.2014.03.134
0013-4686/

[19–23]. Anodic aluminium oxide (AAO) membranes are excellent templates to synthesize nanoscale materials [24–26]. In this paper, one-dimensional nickel nanowires electrocatalyst (NNE) are fabricated with the assistance of AAO membranes for the electro-oxidation of urea. By comparing with bulk nickel film electrocatalysts (NFE), the performance of NNE towards urea electro-oxidation is evaluated, with the intention of improving the oxidation current density, the catalyst stability, and the current efficiency during urea electrolysis.

2. Experimental

2.1. Fabrication of AAO templates

AAO templates were prepared by a two-step electrochemical oxidation of aluminium [27–29]. An aluminum foil (2 cm x 4 cm, annealed, 0.25 mm thickness, Alfa Aesar, 99.99%) and a platinum foil (4 cm x 4 cm) were used as the anode and the cathode in a standard two-electrode electrochemical cell for the fabrication of AAO templates. AAO templates were prepared as followed:

- The Al foil was first sonicated in acetone (Fisher Scientific, 99+ wt%) with a Zenith Ultrasonic bath at 40 kHz for 30 min.
- The Al foil was rinsed with ultrapure water (Alfa Aesar, 99.9 wt%) and immersed in 5 M NaOH (Fisher Scientific, 99.5%) solution for 5 min.
- The Al foil was electropolished in a mixture solution of perchloric acid (Alfa Aesar, 70 wt%) and ethanol (Alfa Aesar, 99.9 wt%) with the volume ratio of 1:4 for 2 min at 20 V in order to create a smooth and homogenous surface for anodization. The temperature of the solution was controlled within 5 °C using an ice water bath throughout the electropolishing procedure.
- The first anodization of the electropolished Al foil was performed in a 2.7 wt% oxalic acid (Alfa Aesar, 5.0 wt%) within 5 °C at 40 V for 4 h.
- After the first anodization, the Al foil was immersed in a mixture solution of 1.8 wt% chromic acid (H_2CrO_4) and 6 wt% phosphoric acid (H_3PO_4) at 60 °C for 60 min to remove the initial oxide on the surface of Al foil.
- A second anodization was carried out under the same operation conditions as the first anodization for a period of 20 h. The temperature of the electrolyte was maintained within 5 °C using an ice water bath during the two-step anodization process.
- Finally, the anodized Al foil was electrochemically treated in a 70 wt% perchloric solution at 45 V for 5 s at room temperature to detach the AAO membrane from the surface of the Al foil. After the detachment step, an AAO membrane was obtained to be used as the template for the fabrication of the NNE.

2.2. Fabrication of the NNE through AAO templates

NNE were fabricated by electrodeposition with the assistance of AAO templates. A Ti foil (Aesar, 99.99%, 0.127 mm thickness) substrate was first polished with 1 μm and 0.05 μm alumina powder and sonicated consecutively for 10 min in acetone and deionized water and then was dried with an Argon gas flow. Before electrodeposition, one side of the AAO template was sputtered with small amounts of gold to improve its conductivity and facilitate the electrodeposition. Conductive carbon paint was used to paste the AAO template onto the surface of the Ti foil in order to minimize the gap between the AAO template and the Ti foil substrate. A typical three-electrode electrochemical cell consisting of a Ag/AgCl reference electrode, a platinum foil counter electrode (4 cm x 4 cm), and the AAO attached working electrode (1 cm x 2 cm), was employed in the electrodeposition experiments. Electrodeposition for NNE was performed at a constant potential of -0.85 V vs. Ag/AgCl for 60 min at room temperature using a Solartron 1470E potentiostat. The electrolyte was prepared by dissolving 30 g of $NiSO_4.6H_2O$, 4.5 g of $NiCl_2.6H_2O$, and 4.5 g of H_3BO_3 in 120 ml deionized water. During the electrodeposition, the electrolyte was stirred at 200 rpm with 25.4 mm x 9.5 mm magnetic stirring bar. After completing the electrodeposition of the nickel nanowires, the working electrode was immersed in 5% NaOH for 2 h to dissolve the AAO template and then was rinsed with deionized water several times. The fabricated NNE were cut into two identical parts (1 cm x 1 cm each) for characterization and electrochemical measurements. Control electrocatalysts/electrodes - bulk nickel film electrocatalysts/electrodes (NFE), were prepared at the same operation conditions that the NNE, except for the electrodeposition time. NFE were only electrodeposited for 6 min to obtain the same loading of nickel as that of the NNE. Since the existence of the AAO template can slow down the transport of nickel ions from the electrolyte to the electrode surface, the fabrication of the NNE needs longer electrodeposition time to obtain the same loading of nickel as that of the bulk NFE. Nickel loadings were determined by atomic absorption spectroscopy (AAS) (AAnalyst 400, PerkinElmer). The nickel on each electrode was dissolved in a 20 wt% HCl solution with 30 min of sonication. The nickel concentration in the solution was measured with the AAS, using a hollow cathode lamp. Nickel loadings of 1.3 ± 0.1 mg·cm^{-2} were achieved for both the NNE and the NFE.

2.3. Characterization

The morphologies of as-synthesized AAO templates were characterized by atomic force microscopy (AFM, Agilent Technologies 5500) under ambient conditions in AC mode with NSC15/AIBS probes from MikroMasch USA (Wilsonville, OR). Scanning electron microscopy (SEM) images of the AAO templates, NNE, and NFE were obtained by using a JEOL-JSM-6390LV instrument. The X-ray diffraction (XRD) pattern of the NNE was collected on a Rigaku Ultima IV X-Ray Diffractometer with monochromatic Cu Kα radiation (λ=0.15405 nm) at a scanning rate of 2° min^{-1}. For the XRD characterization, nickel nanowires were scraped from the titanium substrates.

2.4. Electrochemical measurements

2.4.1. Cyclic voltammetry and chronoamperometry results

The electrochemical activity and stability of the NNE were evaluated in 1 M KOH solution in the absence and presence of 0.33 M urea through cyclic voltammetry (CV) and chronoamperometry measurements. The two electrochemical experiments were carried out in a three-electrode electrochemical cell using a Solartron 1470E potentiostat. A Hg/HgO electrode equipped with a Luggin capillary and a platinum foil (15.0 cm x 20.0 cm) were employed as the reference electrode and counter electrode, respectively. The CV experiments were performed between - 0.1 V to 0.65 V vs. Hg/HgO at a scan rate of 10 mV s^{-1}. In all the cases the sustained periodic state was achieved after 20 sweeps. The chronoamperometry experiments were operated at a constant potential of 0.55 V vs. Hg/HgO for 90 min in an unstirred electrolyte.

2.4.2. Voltage step

Voltage step experiments were performed to quantify the current efficiencies of urea electrolysis at different cell voltages. The voltage step experiments were performed in 1 M KOH solution in the absence and presence of 0.33 M urea stirred at 200 rpm in a two-electrode electrochemical cell by using an Arbin instrument BT-2000. NNE and NFE (1.0 cm x 1.0 cm) were assigned as anodes and a NNE (2.0 cm x 2.0 cm) as the cathode. The cell voltage was stepped from 1.35 to 1.60 V in 25 mV increments with a 30 sec step time. The

range of the cell voltage was determined by the CV experiments described above.

2.5. Gas product analysis

The gases generated at both electrodes were collected separately by using a Hoffman electrolysis cell (Fisher Scientific) with a solution of 1 M KOH in the absence and the presence of 0.33 M urea. The experiments were performed with a NNE anode (1 cm x 1 cm) and a NNE cathode (1 cm x 2 cm) at a constant voltage of 1.55 V and 25 °C for 24 hours. The diagram of the urea electrolysis using the Hoffman electrolysis cell is shown the in supporting information as Figure S1 (a). The composition of the gases was measured using a SRI 8610 C Gas Chromatograph equipped with a TCD detector, a molecular sieve 13X column, and a HayeSep D packed column. Gas samples of 1 mL were manually injected. The oven temperature was held at 51 °C for five minutes followed by a ramp of 10 °C min^{-1} up to 200 °C and then held for five minutes to complete a 23 minutes analysis time. The injector valve and detector temperatures were 140 °C and 102 °C, respectively. Argon was used as the carrier gas with a flow rate of 10 mL min^{-1}. The data was collected and analyzed using PeakSimple chromatography software (SRI instruments).

3. Results and discussion

3.1. SEM and AFM analysis of AAO templates

The as-prepared AAO templates were characterized by Scanning Electron Microscopy (SEM) and Atomic Force Microscopy (AFM). The SEM image (Fig. 1a) shows that the shape, size and distribution of the pores in the AAO templates are uniform with an average pore diameter of ca. 90 nm. The AFM images (Fig. 1b) further indicate that the pore diameters and inter-pore distances in the AAO templates are ca. 90 nm and 130 nm, respectively, which is in agreement with the SEM results.

3.2. SEM and XRD analysis of NFE and NNE

Fig. 2a shows that electrodeposited nickel without the assistance of the AAO template (NFE) only consisted of dense nickel particles with partial agglomeration. However, Fig. 2b displays that electrodeposited nickel with the assistance of the AAO template (NNE) consists of long nanowires with a diameter of ca. 90 nm. As expected, the diameter of the NNE closely corresponds to the diameter of the pores in the AAO template. The crystal structure of the NNE was characterized by X-ray diffraction analysis. Fig. 2c shows three characteristic diffraction peaks indexed as the (111), (200), and (220) planes of face-centered cubic nickel [30,31], which is consistent with the standard card No. 00-004-0850 provided by the international center for diffraction data (ICDD). The XRD pattern does not reveal any impurity peaks, indicating the products are pure nickel.

3.3. Electrochemical analysis

The electrochemical performance of the NNE towards urea oxidation was examined by CV (Fig. 3a) and chronoamperometry (Fig. 3b). In Fig. 3a, curves 1 and 3 exhibit the CVs of the NFE in 1 M KOH in the absence and presence of 0.33 M urea; meanwhile, curves 2 and 4 exhibit the CVs of the NNE in 1 M KOH in the absence and presence of 0.33 M urea at a scan rate of 10 mV s^{-1}. A pair of redox current peaks can be observed in curve 2 due to the reversible transformation between $Ni(OH)_2$ and NiOOH [2,7]. The current density in the presence of urea (curve 4) is much higher than that in the absence of urea (curve 2), indicating that the NNE are effective catalysts towards urea electro-oxidation in the alkaline media. Moreover, curve 4 shows that the oxidation of urea begins approximately at 0.46 V vs. Hg/HgO where NiOOH is formed. The same onset potentials of urea electro-oxidation and the transition from Ni^{2+} to Ni^{3+} suggest that Ni^{3+} are the active sites for urea electro-oxidation [2]. The similar electrochemical phenomenon can be observed as well in curve 1 and curve 3 of Fig. 3a when using NFE as catalysts. However, there was a big difference in the current density due to the urea electro-oxidation (curve 3 and 4 in Fig. 3a) between the two electrodes. It is clear that the NNE produce a much higher urea oxidation current than that of the bulk NFE. The behavior can be attributed to the fact that nanostructured materials have a much larger surface area than their bulk counterparts, which can offer more active sites, promote electron transfer and enhance the current density. In order to validate this statement, the electroactive surface area (ESA) was calculated according to the following equation [9]:

$$ESA = Q/(m\,q) \tag{5}$$

where Q is the charge needed to reduce Ni^{3+} to Ni^{2+} which can be calculated from the CV (curve 1 and curve 2 in Fig. 3a); m is the loading (1.3 ± 0.1 mg.cm^{-2}) of nickel catalyst, and q is the charge associated with the formation of a monolayer of $Ni(OH)_2$. The charge (q) has been reported as 257 μC.cm^{-2}, one electron transferred from Ni^{3+} to Ni^{2+}. The electro-active surface areas of the nickel nanowires catalysts and bulk nickel film catalysts are then calculated as 79.1 cm^2.mg^{-1} and 18.6 cm^2.mg^{-1}, respectively. This confirms that the nickel nanowires catalysts have a larger catalytic surface area than the bulk nickel film catalysts, and thus leads to a higher catalytic activity for urea electro-oxidation.

In order to further evaluate the electrocatalytic activity and stability of the NNE, chronoamperometry experiments of NFE and NNE were performed at a potential of 0.55 V vs. Hg/HgO in 1 M KOH in the absence and presence of 0.33 M urea. NNE produced a continuous, stable and higher current density in 1 M KOH solution in the presence of 0.33 M urea (curve 4 in Fig. 3b), although the current slowly decreases with time. The current in the chronoamperometry experiments usually decays over time mainly associated with the rapid depletion of electro-active species at the electrode surface in an unstirred electrolyte [32]. The chronoamperometry results indicate that (1) both the NNE and the bulk NFE are stable and active electrocatalysts towards urea electro-oxidation and (2) the NNE have higher catalytic activity than bulk NFE, which agrees well with the results of the CV experiments.

Voltage step analyses of the NNE and the NFE are shown in Fig. 4. The voltage step experiments were conducted to evaluate the current efficiency of urea electrolysis on both electrodes by quantifying contribution to the current due to the urea electrolysis at different cell voltages. The experiments were performed in 1 M KOH in the absence and presence of 0.33 M urea, at a 200 rpm constant stirring. The percentages of current density caused by urea electrolysis on both electrodes were calculated and displayed in Fig. 4c. The results demonstrate that NNE can lead to a higher current efficiency in the whole range of cell voltage than bulk NFE. Moreover, the maximum current portion attributed to urea electrolysis on NNE reaches to ca. 76% versus 64% on bulk NFE when the cell voltage is 1.55 V. It means that NNE increase the maximum current efficiency of urea electrolysis by ca. 19% with respect to the NFE. It is hypothesized that the enhanced current efficiency of urea electrolysis is due to the larger surface area of the nanowires, which can decrease the surface blockage of the catalysts, promote electron transfer and thus facilitate urea electro-oxidation. It is noted that different parasitic reactions, such as the oxidation of hydrogen diffusing from the cathode side, may take place in parallel to the urea electro-oxidation reaction on the surface of the anode. However, taking into account that hydrogen also evolves in the absence of urea, and

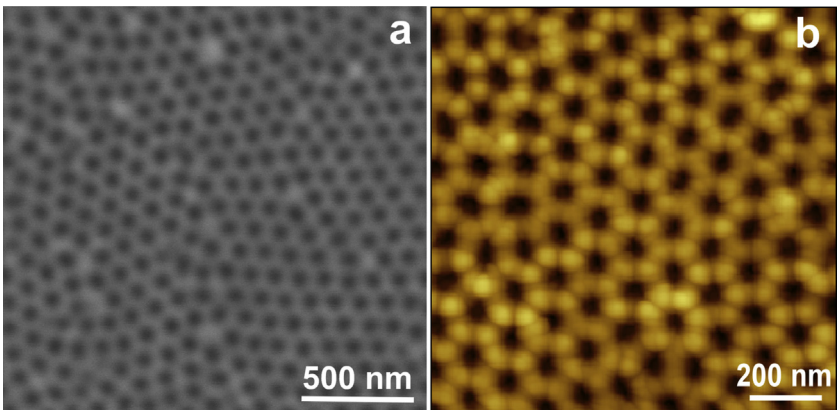

Fig. 1. Characterization of AAO templates. (a) SEM image and (b) AFM image. The characterization results prove that porous AAO templates with uniform nanoscale pore diameters and inter-pore distances were successfully fabricated by a two-step anodization technique.

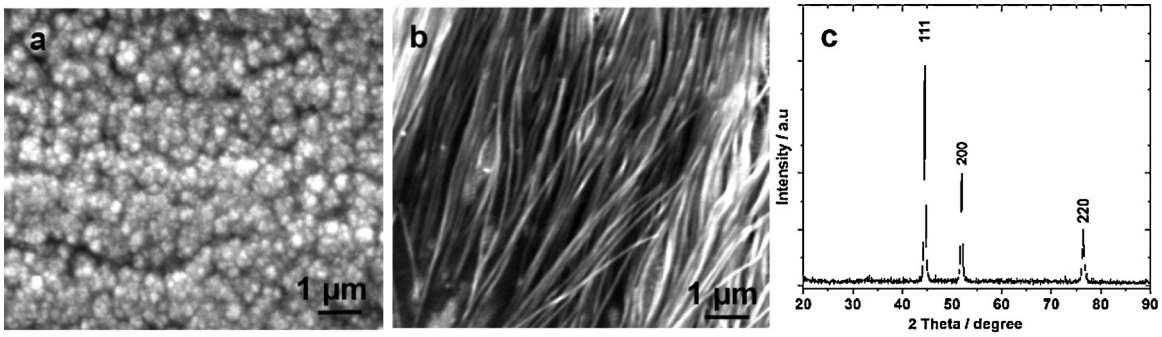

Fig. 2. Characterization of NFE and NNE. (a) SEM image of NFE, (b) SEM image of NNE, (c) XRD pattern of NNE. The NFE consists of dense nickel particles and NNE consists of pure nickel nanowires.

that low concentrations of dissolved hydrogen are expected in the electrolyte, the contributions of this reaction to the measured current density caused by urea electrolysis on both electrodes was subtracted with the current measured in the absence of urea.

3.4. Gas chromatography analysis

Gas chromatography (GC) tests were performed to analyze the composition of the gas products during the electrolysis of urea. Pure H_2 was detected at the cathodic compartment of the cell while N_2 (75.7%), O_2 (19.5%), and H_2 (4.8%) were detected at the anodic compartment. Gas chromatograms of the cathode gas samples after electrolysis in the presence and absence of urea are shown in Figure S1 b and c, respectively. The insets of Figure S1 b and c show the corresponding gas chromatograms of the anode gas samples after electrolysis where traces of hydrogen diffusing from the cathode are observed in the anode gas in the presence (4.8%) and absence of urea (1%). The results confirm that urea electrolysis is well developed (urea oxidation is the main reaction in the anodic compartment of the cell) and water electrolysis (oxygen evolution

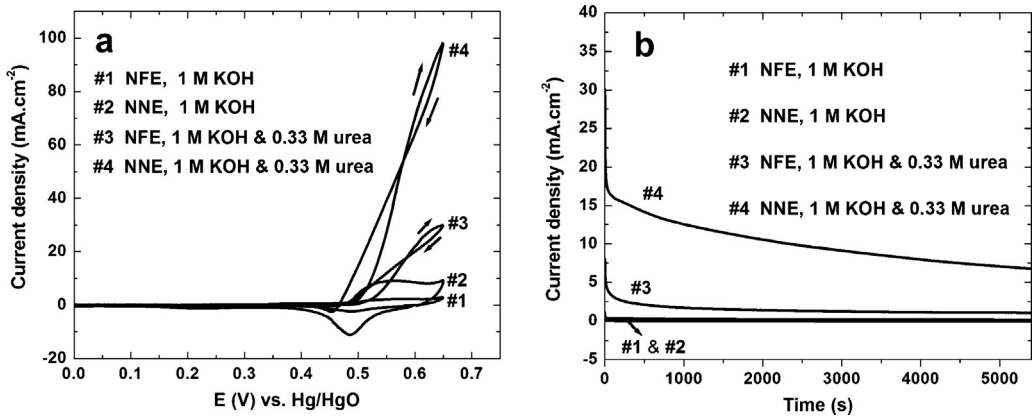

Fig. 3. Cyclic voltammetry (CV) and chronoamperometry of NFE and NNE for urea electro-oxidation. (a) CV of bulk NFE in 1 M KOH solution in the absence (curve 1) and presence (curve 3) of 0.33 M urea (control experiments); CV of NNE in 1 M KOH solution in the absence (curve 2) and presence (curve 4) of 0.33 M urea. The scan rate was 10 mV s^{-1}. (b) Chronoamperometry of bulk NFE in 1 M KOH solution in the absence (curve 1) and presence (curve 3) of 0.33 M urea (control experiments). Chronoamperometry of NNE in 1 M KOH solution in the absence (curve 2) and presence (curve 4) of 0.33 M urea. Applied potential was 0.55 V vs. Hg/HgO. The NNE produce a much higher urea oxidation current than that of the bulk NFE.

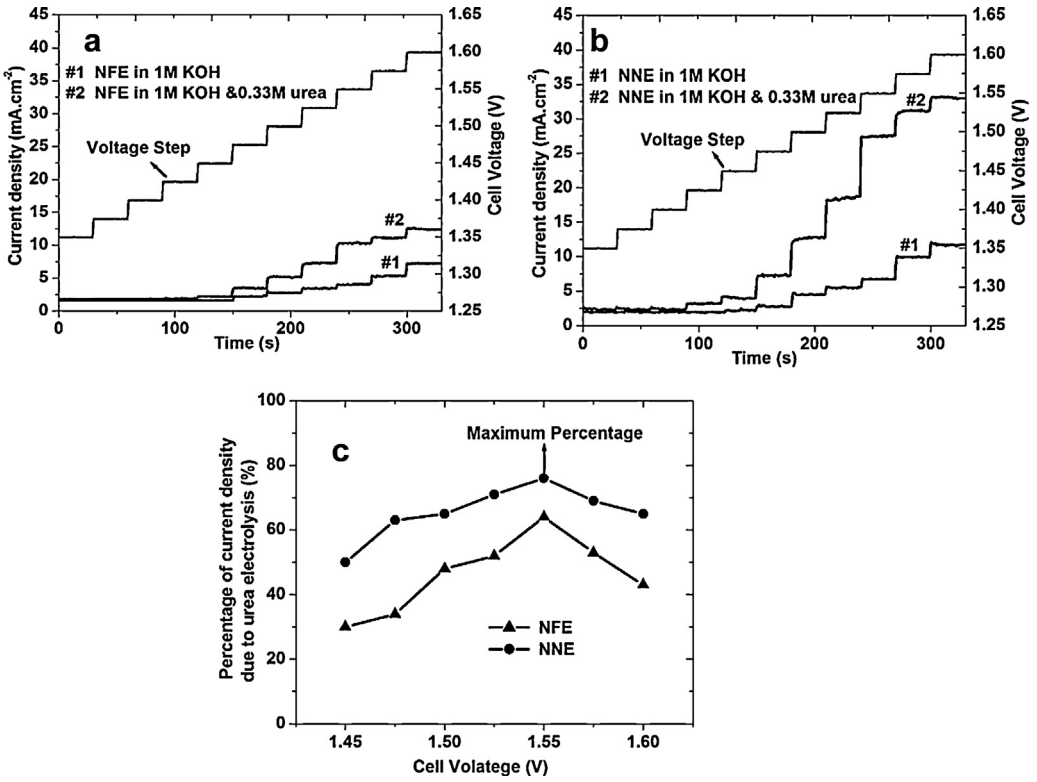

Fig. 4. Voltage step analysis of bulk NFE and NNE. (a) bulk NFE and (b) NNE in 1 M KOH solution in the absence (#1) and the presence (#2) of 0.33 M urea. (c) Percentage of current density due to urea electrolysis at different cell voltages on bulk NFE and NNE. Cell voltage was stepped from 1.35 V to 1.60 V. The current efficiencies of urea electrolysis at different cell voltages on the NNE are enhanced compared to the efficiencies of urea electrolysis on the NFE.

reaction) is suppressed. It is assumed that the presence of urea inhibits oxygen evolution. Carbon dioxide was not found in the anode product gas, the generated carbon dioxide is absorbed in the alkaline electrolyte as a carbonate salt. The small amount of hydrogen detected in the gas in the anodic compartment of the Hoffman cell in the absence and the presence of urea may be due to the hydrogen diffusion from the cathode during the 24 hours electrolysis process.

4. Conclusion

In summary, nickel nanowires were successfully synthesized through electrodeposition using AAO templates. The as-prepared nickel nanowires were characterized by SEM and XRD, and the electrochemical performance of the nickel nanowires for urea electrolysis were measured and analyzed by CV, chronoamperometry and voltage step measurements. When used as catalysts for urea electro-oxidation, nickel nanowires demonstrate higher electrocatalytic activity and higher current efficiency than those of bulk nickel film electrocatalyts. Therefore, nickel nanowires serving as effective catalysts for urea electro-oxidation could lead to new opportunities for hydrogen production and wastewater remediation through urea electrolysis.

Acknowledgment

The authors would like to thank the financial support of the Center for Electrochemical Engineering Research at Ohio University, and the Department of Defense through the U.S. Army Construction Engineering Research Laboratory (W9132T-09-1-0001). The content of the information does not reflect the position or the policy of the U.S. government.

Appendix A. Supplementary data

Supplementary material related to this article can be found, in the online version, at http://dx.doi.org/10.1016/j.electacta.2014.03.134.

References

[1] A.N. Rollinson, J. Jones, V. Dupont, M.V. Twigg, Urea as a hydrogen carrier: a perspective on its potential for safe, sustainable and long-term energy supply, Energy and Environmental Science 4 (2011) 1216–1224.
[2] B.K. Boggs, R.L. King, G.G. Botte, Urea electrolysis: direct hydrogen production from urine, Chemical Communications (2009) 4859–4861.
[3] E.H. Yu, X. Wang, U. Krewer, L. Li, K. Scott, Direct oxidation alkaline fuel cells: from materials to systems, Energy and Environmental Science 5 (2012) 5668–5680.
[4] R. Lan, S. Tao, J.T.S. Irvine, A direct urea fuel cell - power from fertiliser and waste, Energy and Environmental Science 3 (2010) 438–441.
[5] G. Wang, Y. Ling, X. Lu, H. Wang, F. Qian, Y. Tong, Y. Li, Solar driven hydrogen releasing from urea and human urine, Energy and Environmental Science 5 (2012) 8215–8219.
[6] A.N. Rollinson, G.L. Rickett, A. Lea-Langton, V. Dupont, M.V. Twigg, Hydrogen from urea-water and ammonia-water solutions, Applied Catalysis B: Environmental 106 (2011) 304–315.
[7] W. Yan, D. Wang, G.G. Botte, Electrochemical decomposition of urea with Ni-based catalysts, Applied Catalysis B: Environmental 127 (2012) 221–226.
[8] C. Zamfirescu, I. Dincer, Utilization of hydrogen produced from urea on board to improve performance of vehicles, International Journal of Hydrogen Energy 36 (2011) 11425–11432.
[9] D. Wang, W. Yan, S.H. Vijapur, G.G. Botte, Enhanced electrocatalytic oxidation of urea based on nickel hydroxide nanoribbons, Journal of Power Sources 217 (2012) 498–502.
[10] C. Carlesi Jara, S. Giulio, D. Fino, P. Spinelli, Combined direct and indirect electrooxidation of urea containing water, Journal of Applied Electrochemistry 38 (2008) 915–922.
[11] W. Simka, J. Piotrowski, A. Robak, G. Nawrat, Electrochemical treatment of aqueous solutions containing urea, Journal of Applied Electrochemistry 39 (2009) 1137–1143.

[12] D. Wang, W. Yan, G.G. Botte, Exfoliated nickel hydroxide nanosheets for urea electrolysis, Electrochemistry Communications 13 (2011) 1135–1138.
[13] V. Vedharathinam, G.G. Botte, Understanding the electro-catalytic oxidation mechanism of urea on nickel electrodes in alkaline medium, Electrochimica Acta 81 (2012) 292–300.
[14] D.A. Daramola, D. Singh, G.G. Botte, Dissociation Rates of Urea in the Presence of NiOOH Catalyst: A DFT Analysis, Journal of Physical Chemistry A 114 (2010) 11513–11521.
[15] W. Yan, D. Wang, G.G. Botte, Nickel and cobalt bimetallic hydroxide catalysts for urea electro-oxidation, Electrochimica Acta 61 (2012) 25–30.
[16] R.-Y. Ji, D.-S. Chan, J.-J. Jow, M.-S. Wu, Formation of open-ended nickel hydroxide nanotubes on three-dimensional nickel framework for enhanced urea electrolysis, Electrochemistry Communications 29 (2013) 21–24.
[17] R.L. King, G.G. Botte, Investigation of multi-metal catalysts for stable hydrogen production via urea electrolysis, Journal of Power Sources 196 (2011) 9579–9584.
[18] A.T. Miller, B.L. Hassler, G.G. Botte, Rhodium electrodeposition on nickel electrodes used for urea electrolysis, Journal of Applied Electrochemistry 42 (2012) 925–934.
[19] C.-J. Zhong, J. Luo, P.N. Njoki, D. Mott, B. Wanjala, R. Loukrakpam, S. Lim, L. Wang, B. Fang, Z. Xu, Fuel cell technology: nano-engineered multimetallic catalysts, Energy and Environmental Science 1 (2008) 454–466.
[20] E. Yoo, T. Okata, T. Akita, M. Kohyama, J. Nakamura, I. Honma, Enhanced electrocatalytic activity of Pt subnanoclusters on graphene nanosheet surface, Nano Letters 9 (2009) 2255–2259.
[21] R. Wang, C. Xu, X. Bi, Y. Ding, Nanoporous surface alloys as highly active and durable oxygen reduction reaction electrocatalysts, Energy and Environmental Science 5 (2012) 5281–5286.
[22] A. Chen, P. Holt-Hindle, Platinum-based nanostructured materials: synthesis, properties, and applications, Chemical Reviews 110 (2010) 3767–3804.
[23] A. Manthiram, A.V. Murugan, A. Sarkar, T. Muraliganth, Nanostructured electrode materials for electrochemical energy storage and conversion, Energy and Environmental Science 1 (2008) 621–638.
[24] H. Masuda, K. Fukuda, Ordered metal nanohole arrays made by a two-step replication of honeycomb structures of anodic alumina, Science 268 (1995) 1466–1468.
[25] P.-X. Hou, W.-J. Yu, C. Shi, L.-L. Zhang, C. Liu, X.-J. Tian, Z.-L. Dong, H.-M. Cheng, Template synthesis of ultra-thin and short carbon nanotubes with two open ends, Journal of Materials Chemistry 22 (2012) 15221–15226.
[26] Y. Liang, C. Zhen, D. Zou, D. Xu, Preparation of free-standing nanowire arrays on conductive substrates, Journal of the American Chemical Society 126 (2004) 16338–16339.
[27] M.K. McQuaig Jr., A. Toro, G.W. Van, W.Z. Misiolek, The effect of high temperature heat treatment on the structure and properties of anodic aluminum oxide, Journal of Materials Science 46 (2011) 243–253.
[28] S.-C. Lin, Y.-F. Chiu, P.-W. Wu, Y.-F. Hsieh, C.-Y. Wu, Templated fabrication of nanostructured Ni brush for hydrogen evolution reaction, Journal of Materials Research 25 (2010) 2001–2007.
[29] J.H. Yuan, W. Chen, R.J. Hui, Y.L. Hu, X.H. Xia, Mechanism of one-step voltage pulse detachment of porous anodic alumina membranes, Electrochimica Acta 51 (2006) 4589–4595.
[30] H. Niu, Q. Chen, M. Ning, Y. Jia, X. Wang, Synthesis and one-dimensional self-assembly of acicular nickel nanocrystallites under magnetic fields, Journal of Physical Chemistry B 108 (2004) 3996–3999.
[31] F. Tao, Y. Liang, G. Yin, D. Xu, Z. Jiang, H. Li, M. Han, Y. Song, Z. Xie, Z. Xue, J. Zhu, Z. Xu, L. Zheng, X. Wei, Y. Ni, Concentric sub-micrometer-sized cables composed of Ni nanowires and sub-micrometer-sized fullerene tubes, Advanced Functional Materials 17 (2007) 1124–1130.
[32] C.G. Zoski, Handbook of Electrochemistry, Elsevier Academic Press, 2006, pp. 10.